JOINT EUROPEAN TORUS JET

JET–P(89)26

M. Bures, V. Bhatnagar, J.P. Christiansen, G. Cottrell, S. Corti, L-G Eriksson,
T. Hellsten, J. Jacquinot, O.N.J. Jarvis, P. Lallia, P. Lomas, J. O'Rourke,
A. Taroni, C. Sack, D.F.H. Start and JET Team

Enhanced Performance of High Current Discharges in JET Produced by ICRF Heating During the Current Rise

Enhanced Performance of High Current Discharges in JET Produced by ICRF Heating During the Current Rise

M. Bures[1], V. Bhatnagar[1], J.P. Christiansen[1], G. Cottrell[1], S. Corti[1], L-G Eriksson[2], T. Hellsten[1], J. Jacquinot[1], O.N.J. Jarvis[1], P. Lallia[1], P. Lomas[1], J. O'Rourke[1], A. Taroni[1], C. Sack[1], D.F.H. Start[1] and JET Team*

JET-Joint Undertaking, Culham Science Centre, OX14 3DB, Abingdon, UK

[1]*JET-Joint Undertaking, Culham Science Centre, OX14 3DB, Abingdon, UK*
[2]*Chalmers University of Technology, Gothenburg, Sweden*
** See Appendix 1*

Preprint of Paper to be submitted for publication in
Plasma Physics and Controlled Fusion

JET-P(89)26

ENHANCED PERFORMANCE OF HIGH CURRENT DISCHARGES IN JET PRODUCED BY ICRF HEATING DURING THE CURRENT RISE

by

M. Bures, V. Bhatnagar, J.P. Christiansen, G. Cottrell, S. Corti, L.-G. Eriksson*, T. Hellsten, J. Jacquinot, O.N. Jarvis, P. Lallia, P. Lomas, J. O'Rourke, A. Taroni, C. Sack and D.F.H. Start

JET Joint Undertaking, Abingdon, Oxon, OX14 3EA, U.K.

*Chalmers University of Technology, Gothenburg, Sweden

Preprint of an Oral Paper presented at 16th European Conference on Controlled Fusion and Plasma Physics, Venice, Italy, 13th-17th March 1989 and to be submitted for publication in Plasma Physics and Controlled Fusion

May 1989

Table of Contents

1.0 Abstract.

The performance of high current discharges can be improved by applying central ICRF heating before or shortly after the onset of sawtooth activity in the plasma current rise phase. Long sawtooth-free periods have been obtained which result in a transiently-enhanced discharge performance. High $T_e(0) = 9$ - 10.5 keV with peaked profiles $T_e(0)/\langle T_e \rangle = 3$ - 4 were obtained giving values of $n_e(0)T_e(0)$ up to 6 10^{20} (keV m^{-3}). Improvements in $T_i(0)$ and neutron production are observed. A best value of $n_D(0)T_i(0)\tau_E = 1.65\ 10^{20}$ (m^{-3} keVs) was achieved. Local transport simulation shows that the electron and ion thermal diffusivities do not differ substantially in the two cases of current-rise(CR) and flat-top(FT) heating, the performance of the central plasma region being enhanced, in case of current-rise, entirely by the elimination of the sawtooth instability. The maximum D-D reaction rate is enhanced by a factor 2 compared to flat-top value An appreciable part of the reaction rate is attributed to 2nd harmonic deuterium ($2\omega_{CD}$) heating. In all current-rise discharges radiation amounts to 25-50% of total power and Z_{eff} remains roughly constant.

2.0 Introduction.

For optimising the fusion performance of the plasma discharges, simultaneous high values of central plasma parameters, in particular ion density $n_D(0)$ and ion temparature $T_i(0)$, are clearly desirable. The fusion power can also be enhanced by the creation of high energy tail in the distribution of minority particles, as in the T(D) scheme proposed by Stix(1975) and later discussed by Jacquinot(1988) and Cottrell(1989). In this scheme,the minority species is indicated in the bracket, a high value of the $n_e(0)T_e(0)$ product is important in order to optimise the minority energy which should coincide with the maximum of the D-T cross section. There are two ways of improving the performance of the central plasma region. First,it is important to stabilise the sawteeth(Campbell,1988) and to retain the energy stored within the $q = 1$ volume affected by the instability. It is rather easy to lengthen considerably the sawtoothperiod during 2 and 3 MA discharges; however, it proved to be difficult to avoid a high rate of instability during higher current discharges. As described below, the application of RF power during the plasma current-rise phase of 5 and 6 MA discharges results in a long sawtooth-free period and the "Monster" sawtooth regime. Another way of substantially enhancing the central parameters is to reduce the thermal transport in the inner plasma region by pellet injection(Jacquinot 1988, Schmidt 1988) to produce peaked density and temperature profiles. In both these cases a highly

reactive discharge is obtained, based on the improved performance of the inner parts of the plasma.

In this paper we describe and analyse a series of experiments with RF heating during the plasma current rise phase. Another aspect of RF heating during the current rise in the JIPP T-IIU tokamak was discussed by Toi(1987). During those current rise experiments the improvement in global confinement was attributed to the active control of the current profile by applying a current ramp during a steady-state phase of the discharge. As the plasma current has already penetrated, the sawtooth instability was well established and the current ramp was simply driving an edge current.

3.0 Experimental arrangements.

ICRF heating experiments at plasma currents of 5 and 6 MA during the initial current-rise were carried out in the hydrogen minority heating of deuterium plasma with the central toroidal magnetic field B_T =3.1T. The RF antennas were phased as dipoles with maximum power emitted at $k_{||}=7$ m^{-1}. The RF frequency was 48 MHz, which places the cyclotron layer on magnetic axis. RF power deposition calculations indicate a highly localised central heating which can be approximated by a gaussian deposition profile of 20 cm e-folding length. During the 5 MA discharges, the RF power was applied at the level of $I_p=3.7$ to 3.9 MA and was ramped up during 0.5 s to reach the full power at $I_p=4$ to 4.2 MA. During the 6 MA discharges, the corresponding current levels were 4.45 MA at onset of RF power and full power was reached at the level of 4.75 MA. The CR heating data are compared to the flat-top heating data performed for each plasma current during the same day and with the similar conditions of the tokamak. Typical FT target density and Z_{eff} were $<n_e>=2.3$ - 3 10^{19} m^{-3}, $Z_{eff}=1.6$ - 2.5 for 5 MA discharges and $<n_e>=2$ 10^{19} m^{-3}, $Z_{eff} \approx 4$ for 6 MA.

4.0 Experimental results.

4.1 Current penetration and sawtooth behaviour.

During the 5 MA discharges, in the absence of RF heating, the sawtooth activity starts when the plasma current reaches the value 4.6 - 4.7 MA. The application of RF heating delays the onset of sawteeth, the delay increasing with RF power. Fig.1 compares the evolution of the central electron temperature during RF heating to that of the ohmic discharge. A measure of current penetration is shown by polarimetric measurement of the central safety factor q(0). The first sawtooth crash occurs when q(0) is close to unity. While in the ohmic phase, the reduction in $T_e(0)$ by the sawtooth crash is $\approx$ 200eV, it reaches 3 to 3.5 keV in the case of RF heating with 11 MW of RF power. It implies that q is $\approx$ 1 over a substantial part of the plasma core. This is supported by the T_e profile measurements shown in Fig.2a. Electron temperature profile data are based on ECE measurements and are used in subsequent analysis. The inversion radius of the first crash is roughly 40 cm compared to 15 cm in the ohmic case. During the FT heating the value of inversion radius is $\approx$ 50 cm. The values of radii are estimated with respect to the corresponding major radius $R_0 = 3.1$ m at which $T_e(0) = T_e^{MAX}$. In 6 MA discharges the sawtooth activity starts when the plasma current reaches 4 MA, clearly much earlier than during 5 MA discharges.

The difference may be due to higher resistivity from a higher Z_{eff}. The impurity behaviour is discussed in the Sectin 1.5. The current ramp rate is identical in both cases of 5 and 6 MA discharges. With application of RF power a sawtoothfree period was obtained following the normal sawtooth activity. Thus, as demonstrated by these 6 MA results, the dominant physical mechanism responsible for the delay of sawteeth is similar to that of the "Monster" sawtooth stabilisation(Campbell 1988). This is further supported by the local transport simulations and discussed in the Section 1.10. The stabilisation could be due to the presence of fast ions(Pegoraro, 1988). As indicated by polarimetric measurements of the central q(0), the delay of current penetration also contributes to the delay of sawteeth(see Fig.1).

4.2 Enhanced parameters during current-rise heating.

The main observed improvements for current-rise(CR) heating over heating during the current flat-top(FT) can be summarised:

1) a factor of 1.4-1.5 (5MA discharges) and of 1.8 - 2 (6 MA discharges) increase in α, where α is defined by $\Delta T_e(0) = \alpha P_{RF}/n_e(0)$,

2) 10-20% increase in $T_i(0)$ in both 5 and 6 MA discharges,

3) a factor 2 increase in the D-D reaction rate for 5 MA discharges.

The relatively high gain in $T_e(0)$ during 6 MA discharges (shown in Fig.3) is explained by the low $T_e(0)$ values obtained in the FT phase. Such low values may be the consequence of a large plasma volume within the $q=1$ surface and the losses associated with sawtooth instability (Fig.2b). In fact the fully expanded inversion radius in 6 MA FT reaches the value $r=67$ cm. The rate of increase of $T_i(0)$ with $P_{RF}/n_e(0)$ is roughly the same in all cases of FT and CR heating, but

the absolute values are systematically higher in the current rise. The maximum value for $T_i(0)$ reaches 6.2 keV in 5MA and 6.6 keV in 6 MA discharges. In Fig.4 the value of $n_e(0)T_e(0)$ is plotted for two 5 MA discharges during current FT and CR, with $P_{RF} = 11$ MW. A value of 6 10^{20} (keV m^{-3}) has been reached during CR.

With respect to the energy confinement the 10-20% increase in $\Delta W/ \Delta P_{TOT}$ is not a true measure of the incremental confinement time τ_{INC} because during CR at low RF power levels the maximum performance in terms of the central parameters is reached before the stored energy saturates and it is not clear if the $\Delta W/ \Delta P_{TOT}$ is conserved at higher powers than those achieved, i.e., above $P_n + P_{RF} = 15$ MW. A comparison of two identical 5MA discharges with 11 MW of RF power in CR and FT is presented in Figs.5a and 5b. In particular the CR diamagnetic energy, at the point of maximum performance, is 10 -15% higher than the FT value and so is the corresponding confinement time. This rather small improvement in global confinement is a consequence of relatively small volume affected by the sawtooth instability.

The electron temperature peaking ratio $T_e(0)/\langle T_e \rangle$, shown in Fig.6a, reaches values 3.5 - 4.2 during 5 MA CR compared to 3 in 6 MA CR. Density peaking ratios, plotted in Fig.6b, in CR and FT are similar $n_e(0)/\langle n_e \rangle = 1.4$ - 1.6. Central electron pressure 1.5 bar was achieved and electron pressure gradient 2 bar/m was sustained during the CR. Ion contribution to the total pressure was 0.75 bar. The central $\beta = 3\%$.

4.3 Impurity behaviour.

In general, the impurity situation during the discharge depends on the state of tokamak. Following a vacuum leak or after a disruption, the Z_{eff} and the corresponding ion dilution can be rather high. This results from the fact that the impurity source becomes enhanced. During the RF heating it is observed that neutral and impurity influxes generally increase. Because both the deuterium and impurity influxes are roughly proportional to RF power and increase in the same rate, the Z_{eff} does not, under the normal conditions, appreciably change during the RF pulse or as a function of RF power(see Fig.7). However, the initial state at the onset of RF power is important. First the Z_{eff} depends strongly on density(Bickerton 1988) but also on the strength of impurity sources. One way to reduce such sources is high power ^{3}He or ^{4}He discharge cleaning. Another way to reduce the RF induced impurity influxes is to run discharges with appropriate phasing(Bureš 1988) or at higher densities as mentioned above.

In Fig.7 the Z_{eff} is plotted as a function of RF power. The 5 MA discharges have been run at relatively low value of $Z_{eff} \approx 2$. This was achieved by systematic high power ohmic discharge cleaning performed every third or fourth discharge. Also the density was comparatively high when compared to 6 MA discharges(see Fig.8). Because the main impurity in JET is carbon, the ion dilution in case of 5 MA CR and FT discharges was typically $n_D/n_e = 0.8$. In case of 6 MA, $n_D/n_e \approx 0.4$ except for four CR discharges(see Figs.7 and 8) which were run at higher density. As the thermal neutron production is proportional to the square of the deuterium density, the neutron yield is strongly reduced in the 6 MA case. The details of the neutron production are discussed in the Section 1.8 below. The

inverse dependance of Z_{eff} on plasma density during L and H phase of the neutral beam heated(NBI) discharges was discussed recently by Bickerton(1988). A function $Z_{eff} = (2 + 2/\langle n \rangle_{19})$ was found to be a reasonable fit to the presented data. In Fig.9 the Z_{eff} is plotted as a function of volume averaged density. The line representing a $(2 + 2/\langle n \rangle_{19})$ function is shown for comparison and the bars indicate the spread of Bickertons(1988) dataset. Also our data show inverse proportionality of Z_{eff} with the plasma density. However, the datapoints corresponding to discharges with systematic discharge cleaning, and indicated by the dashed line region, represent best performance which is in line with the best results during NBI heating. Taking a single impurity the concentration $\langle n_I \rangle / \langle n_e \rangle = (Z_{eff} - 1)/\{Z_I(Z_I - 1)\}$ can be estimated assuming carbon being the dominant impurity. In case of 5 MA discharges $\langle n_I \rangle / \langle n_e \rangle = 1.5\text{-}3.5\%$ while in 6 MA discharges $\langle n_I \rangle / \langle n_e \rangle = 9\text{-}11\%$. Thus, we conclude that the overall behaviour of impurities does not differ in any way from the general trends already observed previously during the RF heating. The very good performance in terms of Z_{eff} and impurity concentration in 5 MA discharges is result of three major factors. First, the discharges were run at relatively high density, second with clean limiters and walls due to the systematic helium discharge cleaning and third the RF antennas were phased in dipole configuration. This clearly demonstrates that ICRF heating can be performed at high input power levels and at low Z_{eff} if the necessary conditions are met. With respect to radiated power, the fraction P_{RAD}/P_{TOT} ranges between 25 to 50%. The strongest correlation of P_{RAD}/P_{TOT} was found with density.

5.0 Discussion of RF heating.

5.1 RF power deposition.

The RF heating scenario used in the experiments is hydrogen minority in deuterium. The hydrogen concentration defined $n_H/(n_H+n_D)$ was measured using the low energy neutral flux data from neutral particle analyser. During the 5 MA dicharges, the concentration was typically in the range 5-7%. Consider the 5 MA CR discharge with 11 MW of RF power. At the onset of the RF pulse, the parameters of the discharge and the antenna phasing(toroidal dipole) imply $\approx$65% absorption per pass. Most of this power is absorbed by hydrogen minority due to the fundamental cyclotron absorption while about 10% is damped on electrons by Landau and TTMP damping. The second harmonic damping on deuterium amounts only to 3%. As the minority tail forms, it saturates on a time scale of the Spitzer's slowing down time. t_s is roughly 0.5 sec which is comparable to the time during which the RF power is ramped up to its full value. Shortly after the power reached its maximum the estimate of the effective perpendicular tail temperature, using the Stix's formalism{Stix 1975} and assuming a uniform power density within a central plasma volume of 10 m^3, results in a value $T_{eff}\approx$400 keV. The corresponding parallel temperature is much lower and the estimate{Stix 1975, Andersson et al. 1987} indicates that $T_{II}\approx$25

keV. Recalculating the power absorption including the effects of $T_{\parallel}$ of tail, it becomes >90%, indicating practically complete damping of the launched wave in a single pass. The increase in damping is fully accounted for by enhanced damping on the minority ions. The ratio of power damped by $2\omega_{CD}$ to power going into hydrogen is $P_D/P_H=0.04$. As the pulse progresses in time both electron temperature and density increase. As a result, the slowing down time slightly increases, $t_s=0.55$s. Disregarding the parallel temperature of the tail the absorption per pass is now $\approx$85%. Also at this time the tail temperature has increased somewhat. Including the enhanced absorption by the $T_{\parallel}$ effects of hydrogen tail($T_{\parallel}\approx$45keV) the absorption is practically complete in one pass, >90%. The relative damping by different plasma species is somewhat different compared to what it was at the onset of RF power. 70% is absorbed by hydrogen(60% without $T_{\parallel}$ effects), 13-14% by electrons and 10% by deuterium. The fraction P_D/P_H increased to 0.14. This reflects the consequence of increased ion temperature. For comparison, a similar 5MA discharge with 11 MW of RF power during FT phase was analysed. As in the CR phase the most of the power goes into hydrogen and only 6-7% is absorbed by deuterium. The absorption is practically complete in the first pass. Also the evolution of coupling resistance trace in time does not show any sign of eigenmodes which implies a high damping rate per pass. Its value is in the range of 3Ω. The ratio P_D/P_H is 0.08 which is lower than in CR due to the lower deuterium temperature.

To calculate the power deposition profiles and the power transfer from the fast hydrogen and deuterium to the background plasma species, later used in the transport simulations, a self-consistent code calculation of RF power deposition and the velocity distributions of the hydrogen and deuterium was used{Eriksson

et al. 1989}. The complete spectrum of the dipole antenna was used. The resulting power distribution profiles are plotted in Fig.10. During the CR the power going into electrons decreases and correspondingly the ion heating increases. This results from the competition between the hydrogen and deuterium absorption. Interestingly, the FT electron profile is slightly more peaked and the power transferred to ions is higher than in CR. The slight difference in the electron profile can be understood in terms of broadening of the hydrogen minority damping zone around its cyclotron resonance. This broadening is, in turn, due to the higher parallel temperature of the hydrogen tail.

5.2 Fast particles.

The high energy tails are formed as a result of fundamental cyclotron heating of hydrogen and $2\omega_{cD}$ heating of deuterium. This is indicated by the neutral particle spectra measurements which show the formation of hydrogen and deuterium tails after the application of RF power. It should be stressed that the measured neutral spectra shown in Fig.11 do not provide an exact distribution function of protons and deuterons in the plasma centre. The neutral flux is weighted by the charge-exhange cross section and the particular spectrum represents only one line of sight. Nevertheless a number of qualitative features can be observed. During the 5 MA CR discharge with 11 MW of RF power the hydrogen spectrum develops a tail as shown in Fig.11a. From the theoretical considerations it is expected that, in the centre of the discharge, almost the entire minority population is in the high energy range with an effective temperature well above the measured range. In contrast, for the deuterium distribution function, the theoretical estimates based on the power damped by the deuterons by the

second harmonic damping suggest that, only a fraction of particles should be in the high energy range. This is indeed observed and the measured energy range up to 45 keV for deuterium is appropriate for the anticipated tail temperature as roughly indicated in Fig.11b. The information concerning the hydrogen tail is much more of qualitative nature and, in particular, the true tail temperature is much higher.

Neglecting energy transfer to the ions the energy contained in the fast particles in steady-state distribution can be expressed $P_{FAST}t_s/2$ where P_{FAST} is the RF power coupled to the fast particles and t_s is the minority slowing-down time on the electrons. The energy content of the fast particles can reach a significant level in JET, as discussed earlier by Jacquinot et al.(1988) and Thomas et al.(1988), and is therefore important to include when estimating the confinement time. The anisotropic energy contribution from the fast particles can be estimated from the data obtained with the diamagnetic loop together with data on the electron temperature and density profiles, central ion temperature and Z_{eff}. During the FT heating phase the anisotropic energy can also be obtained from the difference of the diamagnetic energy and the energy estimates based on the equilibrium measurements, i.e., $W_A = 4/3(\Delta W_{DIA} - \Delta W_{MHD})$ as discussed by Christiansen(1987). In Fig.12 the measured anisotropic energy $W_A = 2/3(\Delta W_{DIA} - \Delta W_{KIN})$ is plotted versus $P_{RF}t_s(0)/2$ during the FT heating. A satisfactory correlation is found and W_A scales linearly with $P_{RF}t_s(0)/2$. However the $P_{RF}t_s(0)/2$ is only a rough measure of the fast energy content. It assumes that all RF power is coupled to the minority species in the centre of the discharge, neglects the power transfer to the bulk ions and assumes the infinite confinement of the fast ions. Taking into account all these effects {Eriksson et al. 1989} a rather accurate agreement between the

measured W_A and theoretical estimate can be obtained. The remaining difficulty associated with such calculation is the uncertainty about the ion tail behaviour during the sawtooth crashes and the assumptions about the fast particles confinement. The data set in Fig.12 is not corrected for the offset at $P_{RF}=0$ which is within the error bar of the stored energy measurements. In the CR phase the estimates of W_A cannot be done because the plasma is not in equilibrium and the ΔW_{DIA} and ΔW_{KIN} increments cannot be measured without making rather crude assumptions about the plasma energy evolution due to the ohmic power input. Thus, bearing in mind that the fast energy is proportional to the minority slowing-down time, it is reasonable to conclude that during CR phase its contribution to W_{DIA} is larger than in FT.

5.3 Second harmonic heating.

A summary of the D-D reaction rate data is shown in Fig.13 As explained below, a significant contribution to the neutron enhancement results from the creation of a high energy deuterium tail. The reason why the 6 MA discharges did not produce a comparable improvement is the relatively high Z_{eff} (Fig.7), as discussed in the previous Section 1.5. The correlation between the fluxes of high energy neutrals and neutrons, as plotted in Fig.14, suggests that $2\omega_{CD}$ heating is important in accounting for the observed neutron rate. The low energy channels do not exhibit such a correlation.

To evaluate the importance of the $2\omega_{CD}$ heating for the neutron yield, the self-consistent calculations described in the Section 1.6 were carried out to estimate the nonthermal contribution. Fig.15 compares the results from these

calculations with the measured neutron yield. The open circles represent the simulation of the thermal part of the yield. For the ion temperature profile was assumed that it has the same radial dependence as the electron temperature profile. This assumption is justified by the $T_i(r)$ neutral particle measurements performed on a similar discharge. A very reasonable agreement with the measured values is obtained and the difference can certainly be accounted for by the details of the profiles as well as the details of the theoretical treatment. The contribution from the fast deuterons is indicated. The characteristic peaking of neutron yield as a function of time was previously observed during "Monster" sawtooth discharges with sufficiently long, > 1s, quiescent period. This supports the argument that a finite time is necessary to develop a 2 ω_{CD} tail and also that fast deuterons are lost from the plasma centre during the normal sawtooth activity. The fact that it takes long time to form the deuterium tail may not be surprising because the corresponding slowing-down time is twice the slowing-down time of protons.

The foregoing interpretation can be tested by inspection of the neutron energy spectra and their self-consistent analysis along with the instantaneous neutron yields and the neutron emission radial profiles. The analysis adopts the central ion temperatures provided by the x-ray crystal spectrometer and the n_D/n_e value derived from vissible bremstrahlung measurements of Z_{eff}. The neutron spectra are fitted to a calculation which assumes two distributions, one due to thermal neutron emission corresponding to the bulk ion temperature and a second corresponding to an anisotropic temperature of 30 keV which simulates the 2 ω_{CD} heating. The free variable in this fitting is the fraction of the neutron emission attributable to the RF tail. Unfortunately, the neutron spectra were acquired

over 1-s intervals so that the emission peak indicated in Fig.15 would be observed by the spectrometer as a mean enhancement of only 20%. This neutron analysis produces a 2 ω_{CD} fraction of $18 \pm 9\%$ for the time interval 46-47 s, in good agreement with expectation. However, a fraction of 16 $\pm 8\%$ is similarly indicated for the period 45-46s. The analysis also indicates, that the tail is lost after the crash at 46.9s. Finally, the data support the measured Z_{eff} which were discussed in Section 1.5. The FT discharge neutron spectra are best fitted with a RF tail of 5%.

6.0 Energy confinement.

6.1 Aspects of global confinement.

In this Section some aspects of the global confinement are discussed first. In particular a quantitative estimate of the energy loss due to a sawtooth crash is carried out and the impact of these losses on the incremental confinement time. Later the central energy balance is discussed in terms electron, ion and the fast minority energy balances relevant to the central parts of the discharge where the RF power is deposited. The local transport simulations by means of a code are refered to the next Section.

It was reported previously by Bhatnagar et al.(1988) that the τ_{INC} does not increase for $I_p > 3$ MA. Typically, its saturated value of 350 ms is obtained for $I_p = 3\text{-}3.5$ MA and $q_{CYL} \approx 3.3$. For higher currents τ_{INC} either decreases or remains saturated. To understand the nature of the improved performance during CR the FT data are studied first. In both cases of 5 and 6 MA discharges the plasma energy W_{DIA}, measured by the diamagnetic loop, exhibits the off-set linear behaviour with no dependence on the plasma current. Actually for the same power input the energy content, total confinement time and the corresponding τ_{INC} are same for the both currents. In particular, $\tau_{INC} = 330\text{-}350$ ms. The lack of

I_p dependence is generally believed to be due to the losses associated with sawtooth instability affecting the plasma volume within the $q=1$ surface. In 6 MA FT the inversion radius has expanded to $r \approx 67$cm with the corresponding $R_0 = 3.1$ m. It is easy to make a rough estimate of the energy lost from $q=1$ volume on each sawtooth collapse. It becomes

$$\Delta W^{ST} = (3/2)\pi^2 R_0 n_e(0) r_{INV}^2 \kappa\{\Delta T_e(0)^{ST} + \Delta T_i(0)^{ST} (6-Z_{eff})/5)\}$$

where $\Delta T_{e,i}(0)^{ST}$ are the sawtooth amplitudes of central electron and ion temperatures, r_{INV} is the sawtooth inversion radius, κ is the elongation and $n_e(0)$ is the central electron density. The temperature profiles are assumed to be parabolic within the $q=1$ volume and the density is considered constant. For the ion dilution, carbon is taken to be a dominant impurity. Two discharges were studied with total power input $P_\Omega + P_{RF} = 13.2$ MW. In the 6 MA discharge a marginally higher total energy content(0.3-0.4 MJ) can be explained by a higher fast-particle content, as discussed in the Section 1.7. The radiated power is higher in the 5 MA discharge, i.e.,$P_{RAD}^{5MA} = 6$ MW as compared to $P_{RAD}^{6MA} = 4.5$ MW. In the case of the 5 MA discharge, $\Delta W^{ST} \approx 0.5$ MJ and for the 6 MA discharge the corresponding value is $\Delta W^{ST} \approx 0.7$ MJ. Taking the time average of the central energy and assuming a linear rise during the sawtooth period, the effective loss from the $q=1$ volume $< \Delta W^{ST} >_{time}$ becomes half of the values quoted above. Assuming that the plasma could retain this energy, there would be an increase of $\tau_{INC} = 30$ ms for the 5 MA and 40 ms for the 6 MA discharge. However if we could stabilise the central zone and eliminate the sawtooth instability, the gain would certainly be even larger because the central electron and ion temperatures are not saturated at the time of sawtooth collapse. Whether the resulting

improvement would be sufficient to regain the favourable current scaling observed for $I_p < 3.5$ MA remains uncertain. With respect to CR, as mentioned in the previous Sections, the improvements in the plasma parameters are related to the central part of the plasma that is affected by the sawtooth instability. The improvement in total stored energy is rather small, as can be seen in Fig.5b. In CR, the concept of incremental confinement is not very useful for the power range obtained in the present set of experiments because, for the low power input, the maximum values of ion and electron temperatures in the plasma centre are reached before the total stored energy saturates. To assess whether the global confinement can be substantially increased by heating in CR, higher power has to be coupled to the plasma. This has to await future experiments.

6.2 Central plasma confinement.

The details of $T_e(0)$ time evolution in CR(Fig.1) show some interesting features. In particular the $dT_e(0)/dt$ changes abruptly around $t=45$s and $t=46.8$s. The same behaviour is observed on central electron pressure evolution, see Fig.4; on plotting the total pressure, $p(0) = p_e(0) + p_i(0)$, the abrupt changes are even more accentuated. While the change in $dp(0)/dt$ at 45 s can be explained by the change of the current ramp rate dI_p/dt, the change of the slope at 46.8 s does not seem to be correlated to the ohmic power input. To estimate the magnitude of the central energy loss attributable to this phenomenon the energy density equations, which describe the energy balance at the plasma centre, are written in following form:

$$\frac{dW_e}{dt} + q_{e,i} + \frac{W_e}{\tau_e} = \frac{W_{MIN}}{\tau_{Se}} + p_\Omega + p_{RF}^e$$

$$\frac{dW_i}{dt} - q_{e,i} + \frac{W_i}{\tau_i} = \frac{W_{MIN}}{\tau_{Si}}$$

$$\frac{dW_{MIN}}{dt} + \frac{W_{MIN}}{\tau_S} + \frac{W_{MIN}}{\tau_{MIN}} = p_{RF}^{MIN}$$

Here $W_e = 3/2 n_e T_e$, $W_i = 3/2 n_i T_i$, W_{MIN} is the averaged energy of the minority species including the fraction of deuterons accelerated by $2\omega_{CD}$ heating. $q_{e,i}$ is the equilibration power, τ_e, τ_i, τ_{MIN} represent the electron, ion and minority confinement. $\tau_S = \tau_{Se}\tau_{Si}/(\tau_{Se} + \tau_{Si})$ is the effective slowing-down time including the elecron and ion contributions. Finally, p_Ω is the ohmic power density, p_{RF}^e is the RF power absorbed directly by electrons due to Landau and TTMP damping and p_{RF}^{MIN} is the RF power absorbed by the hydrogen cyclotron and deuterium $2\omega_{CD}$ damping. The radial profiles of redistributed RF power plotted in Fig.10 correspond to $p_{electrons} = p_{RF}^e + W_{MIN}/\tau_{Se}$ and $p_{ions} = W_{MIN}/\tau_{Si}$. Assuming that the minority has reached the steady-state $dW_{MIN}/dt \approx 0$, and with $W = W_e + W_i$ the central confinement can be expressed

$$\frac{W}{\tau_E} = p_\Omega + p_{RF}^{TOT} - \frac{W_{MIN}}{\tau_{MIN}} - \frac{dW}{dt}$$

The change of the slope dw/dt at t=46.8 sec corresponds to an effective central loss $dw/dt \approx 0.1$ Wcm^{-3} which should be compared to the RF power density

plotted in Fig.10. As neither ohmic nor RF power input vary at this time, the observed degradation of central pressure must be due to some instability occuring within the q=1 volume. It might be linked to the onset of sawtooth instability as this loss can be observed at different RF power levels, central pressure levels and different times(see Fig.1), but always just before the first sawtooth crash. This also indicates that the loss is not related to the minority confinement W_{MIN}/τ_{MIN}.

As mentioned above, the major improvement in discharge performance in CR is confined to the central region. This is illustrated in Fig.3. The plotted dependence can be expressed, using the central electron balance equation, in the following form:

$$n_e T_e/p^{TOT} = (2/3)\tau_e\{1 - (W_{MIN}/\tau_{MIN} + W_{MIN}/\tau_{Si} + q_{e,i})/p^{TOT}\}.$$

It immediately follows that, in both 5 and 6 MA CR, the central electron confinement τ_e has to improve because the ion heating W_{MIN}/τ_{Si} does not change significantly and the electron-ion equipartition is reduced only slightly in the higher T_e CR discharges. Similarly, the $T_i(0)$ dependence on $P_{TOT}/n_e(0)$ indicates that the central ion confinement τ_i is improved. This can be seen from the central ion balance

$$n_e T_i/p^{TOT} = (2/3)(n_e/n_i)\tau_i(W_{MIN}/\tau_{Si} + q_{e,i})/p^{TOT}$$

and the same arguments about the ion heating ,as above, apply here. Thus the main question to be answered can be formulated as follows: can the

improvements in the central τ_e and τ_i be simply explained by the elimination of losses associated with sawtooth crashes or does the non-steady state imply additional enhancement? To answer this question we have to await the comparison with a "Monster" stabilised FT discharge at 5 or 6 MA.

6.3 Local transport simulation.

Good insight into the nature of the improvement can be obtained by a localised transport-code simulation. Here we use the Rebut-Lallia model{Rebut et al. 1988} in the $1^{1/2}$-D transport code. The electron and ion transports are solved separately and the current penetration is simulated by the neoclassical resisitivity. The density, temperature profiles and Z_{eff} are taken from the existing JET data base. Two discharges, plotted in Fig.5a and 5b, are compared in CR and FT phases. The calculated power deposition profiles, shown in Fig.10, are used as an input. Time evolution of the plasma parameters are well simulated within 10% of measured values. In the first 0.5-1.0 s, when the RF power is ramped up, the power input has to be slightly reduced to avoid "overshoot" of the simulated $T_e(0)$. By this means, the formation of a minority tail is simulated. Individual sawtooth crashes during the FT are not simulated so that within the $q=1$ volume the conductivities are enhanced above the values predicted by Rebut-Lallia theory to model the sawteeth averaged values of central electron and ion temperatures. The resulting radial profiles of electron and ion diffusivities are plotted in Fig.16 at the time $t=51.0$ sec in FT and 46.5 sec in CR. There is no difference in $\chi_{e,i}$'s outside $r/a=0.45$. Within this radius the CR diffusivities are reduced to values expected for a "Monster" like discharge. Also the radial dependence is as usually observed during such discharges, as discussed by

Taroni(1988). Despite the error bars associated with the accuracy of the measurements, the results seem to indicate that, for this type of 5 MA discharge the ion diffusivity is in the range $0.7 < \chi_i < 1.0$ m²/sec. This value and the ratio $\chi_i/\chi_e \approx 0.5$ are at the lower end of the range generally observed in the previous simulations{Taroni et al.1988} of the "Monster" type discharges at lower plasma currents $I_p < 3.5$ MA and suggest the importance of plasma current for the scaling of heat conductivities. The values of $\chi_{e,i}$'s within $r/a = 0.1$ and outside $r/a = 0.85$ are not reliable due to uncertainties in the profiles and radiated power. The measured and calculated $T_e(r)$ profiles together with computed $T_i(r)$ are plotted in Fig.17. The calculated ion temperature profile is very similar to the profile measured for a similar shot and outside the $q = 1$ surface is very close to the $T_e(r)$.

7.0 Conclusions and discussion.

Elimination of sawtooth activity by the application of high power ICRF heating during the plasma current-rise phase of 5 and 6 MA discharges results in a transiently enhanced performance in terms of all major plasma parameters and, in particular, of central electron and ion temperatures. A high value of $n_e(0)T_e(0) = 6\ 10^{20}$ (keV m^{-3}) has been reached during CR with 11 MW of RF power which is the same as recently achieved with combined RF heating and pellet injection into a 3 MA discharge{Schmidt 1988, Milora 1989}. Neutron yield enhanced by $2\omega_{CD}$ was observed. The electron temperature peaking, $T_e(0)/<T_e>$, reaches the value 4.2 which is a factor 2 higher than in the flat-top phase. The density peaking ($n_e(0)/<n_e> = 1.5$) remains unchanged. No impurity accumulation is observed. The global confinement is improved only marginally and can be entirely accounted for by the retention of energy otherwise lost by sawtooth activity. During the CR the heat diffusivities outside the inversion radius do not seem to be reduced when compared to the values during FT heating but indicate a favourable scaling with the plasma current. The CR heated discharge appears to have the character of a "Monster" stabilised discharge. It is a good candidate for T(D) operation{Jacquinot 1988}, eventually to be combined with pellet injection. It also provides an interesting target for NBI

heating. The possibility of extending this mode of operation for longer period at higher power input levels will be a subject of future experiments.

8.0 Acknowledgements.

We wish to thank our colleagues in the JET team, especially the Tokamak operating teams and those operating the diagnostics used in the experiments reported in this paper.

9.0 References.

1. Anderson D. et al., Nucl. Fusion 27 (1987) p.911.
2. Bickerton R.J. and JET Team, 12th Int. Conf. on Plasma Phys. and Contr. Nucl. Fus. Res., Nice(1988), IAEA-CN-50/A-1-3.
3. Bhatnagar V.P. et al., Proc. 15th Europ.Conf. on Contr.Fusion and Plasma Heating, Vol.12B, Part I, Dubrovnik(1988)358.
4. Bureš M. et al., Plasma Phys. and Contr.Fus., Vol.30, No.2(1988), p.149.
5. Campbell D.J. et al., Phys.Rev.Letters, Vol.60,No 21(1988)2148.
6. Christiansen J.P., J. Comp. Phys. 73(1987)p.85.
7. Eriksson L.-G. et al., to be published in Nuclear Fusion.
8. Jacquinot J. et al., Plasma Phys. and Contr. Fus., Vol.30, no.11, p.1467.
9. Milora S. et al., Proc. 16th Europ.Conf. on Contr.Fusion and Plasma Heating, Vol.13B, Part I, Venice(1989)91.
10. Pegoraro F. et al., 12th Int. Conf. on Plasma Phys. and Contr. Nucl. Fus. Res., Nice(1988), IAEA-CN-50/D-4-6.
11. Rebut P.H., P.P.Lallia and M.L.Watkins, 12th Int. Conf. on Plasma Phys. and Contr. Nucl. Fus. Res., Nice(1988), IAEA-CN-50/D-4-1
12. Schmidt G. et al., 12th Int. Conf. on Plasma Phys. and Contr. Nucl. Fus. Res., Nice(1988), IAEA-CN-50/A-7-1.
13. Stix T.H., Nucl. Fusion 15, (1975) p737.

14. Taroni A. et al., 12th Int. Conf. on Plasma Phys. and Contr. Nucl. Fus. Res., Nice(1988), IAEA-CN-50/A-7-1.

15. Thomas P. and JET Team, 12th Int. Conf. on Plasma Phys. and Contr. Nucl. Fus. Res., Nice(1988), IAEA-CN-50/A-4-4.

16. Toi K., et al., Proc. 14th Europ.Conf. on Contr.Fusion and Plasma Heating, Vol.11D, Part I, Madrid(1987)302.

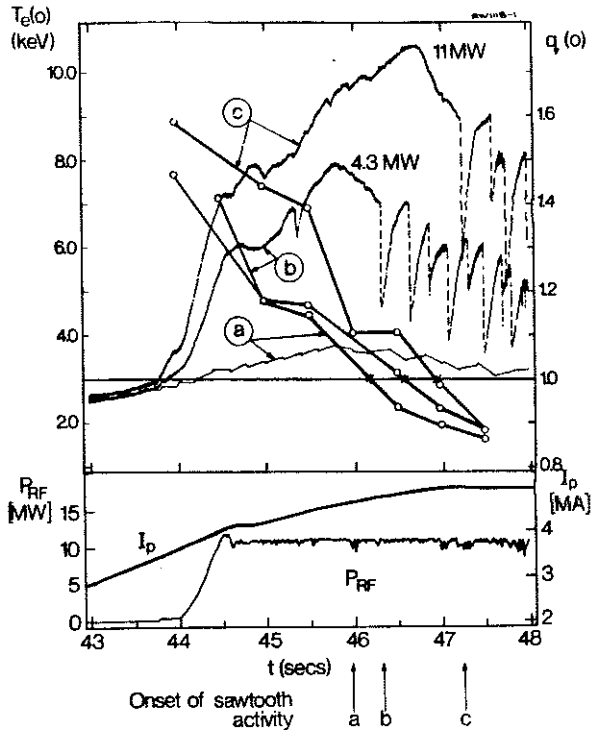

Fig. 1 Central electron temperature and $q(0)$ time evolution in (a) ohmic, (b) $P_{RF}=4.3$ MW and (c) $P_{RF}=11$ MW discharges. The onset of sawtooth instability in the ohmic discharge was deduced from the central soft X-ray channel. Plasma current and RF Power are also shown.

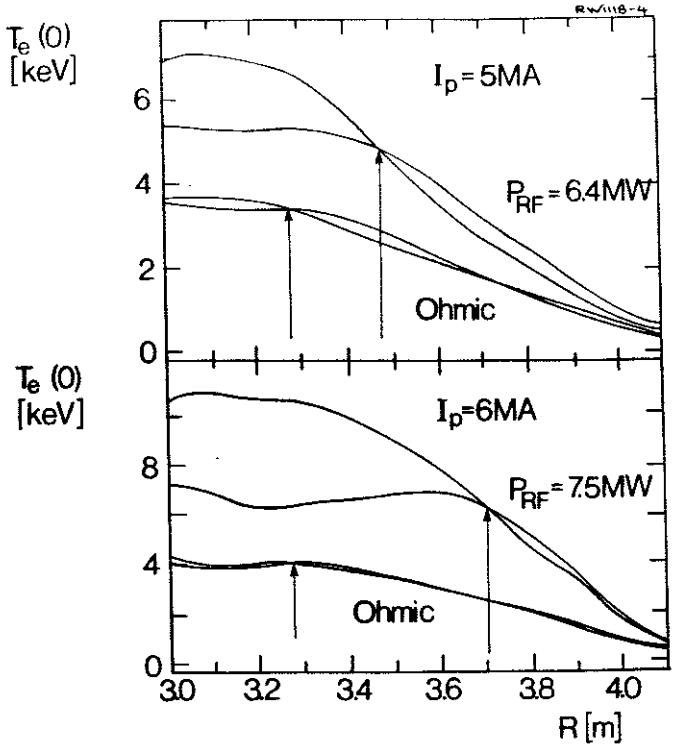

Fig. 2a,b Electron temperature profiles associated with the first sawtooth collapses (just before and after) in ohmic and RF heated discharges in CR. The arrows indicate the inversion radii.

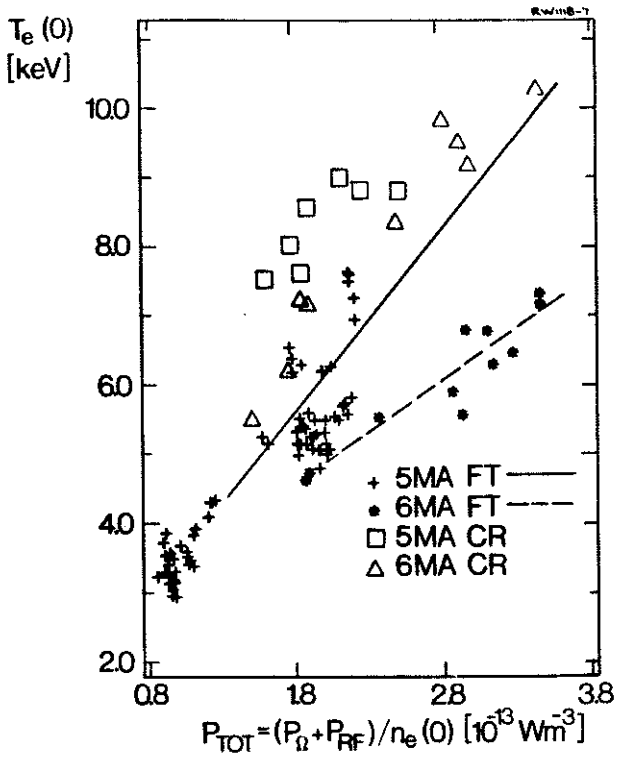

Fig. 3 Central electron temperature versus total power per particle. The full and broken lines are drawn in order to facilitate the reading of the diagram.

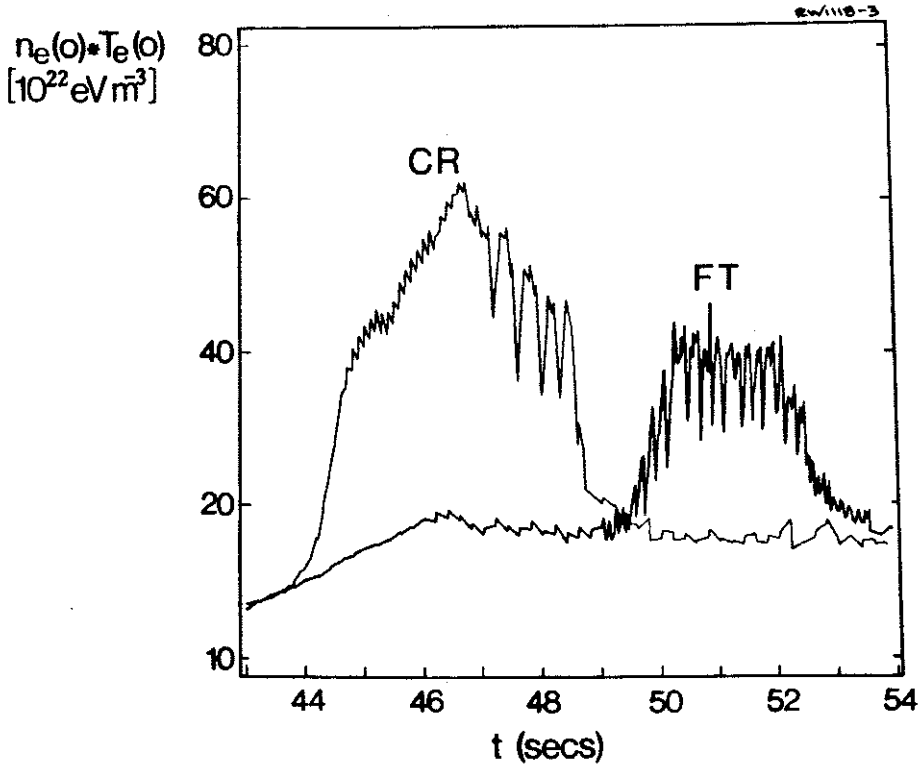

Fig. 4 $n_e(0)T_e(0)$ during CR and FT 5 MA discharges, $P_{RF}=11$ MW.

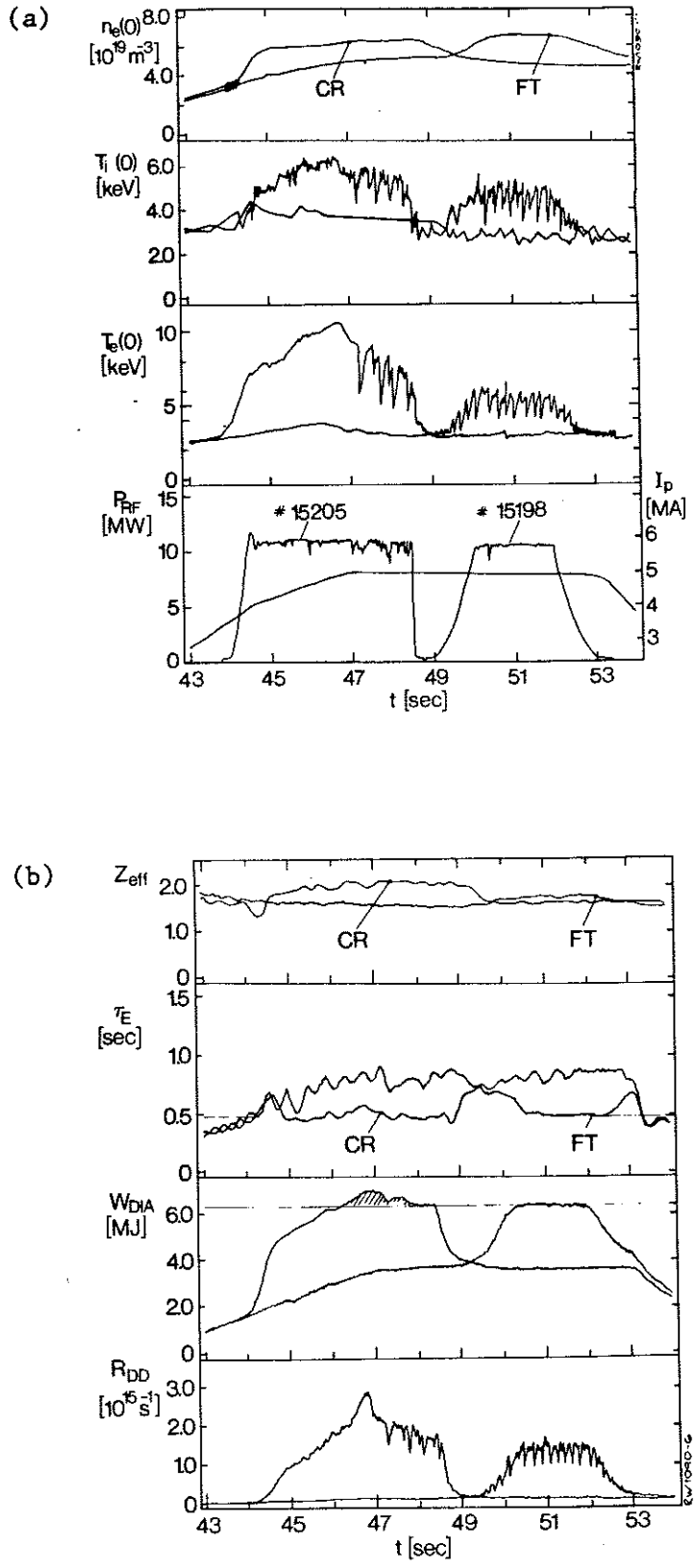

Fig. 5a,b Comparison of two 5 MA discharges in CR and FT. Traces of central electron density, ion and electron temperature, RF power, effective charge, global energy confinement time, diamagntic stored energy and neutron yield are plotted as a function of time.

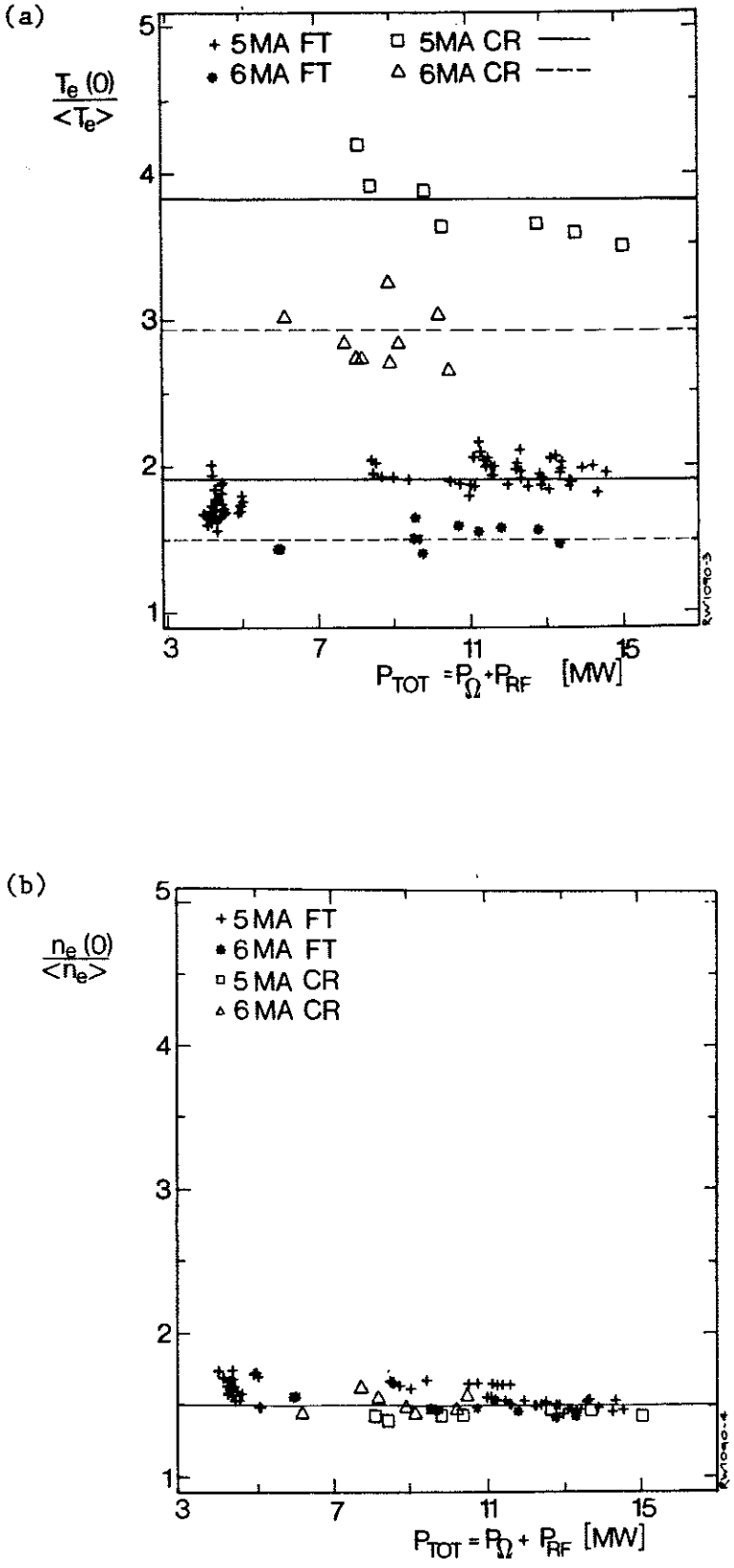

Fig. 6a,b Electron temperature and density peaking factors as a function of input power. The full and broken lines are drawn in order to facilitate the reading of the diagram.

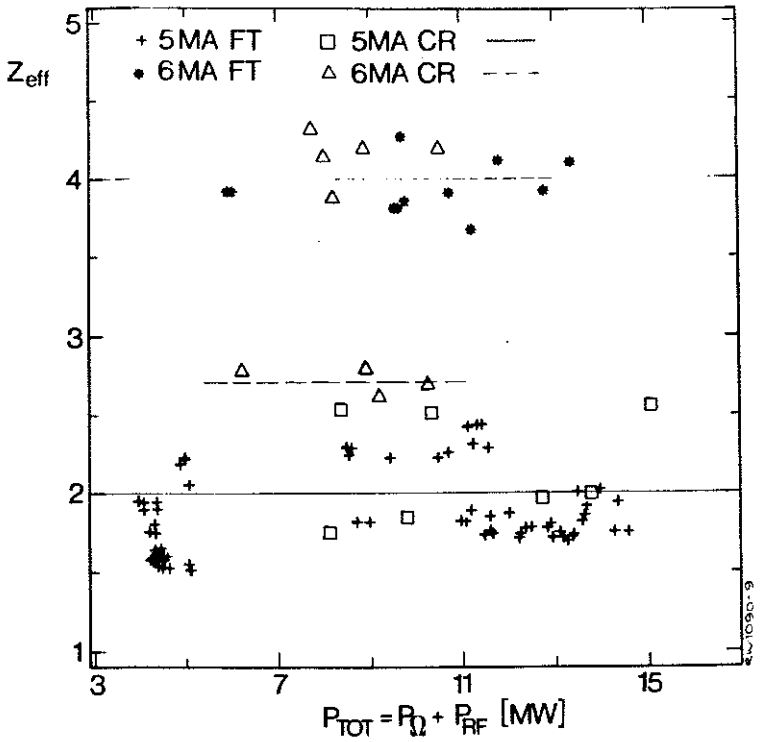

Fig. 7 Effective charge as a function of input power. The full and broken lines are drawn in order to facilitate the reading of the diagram.

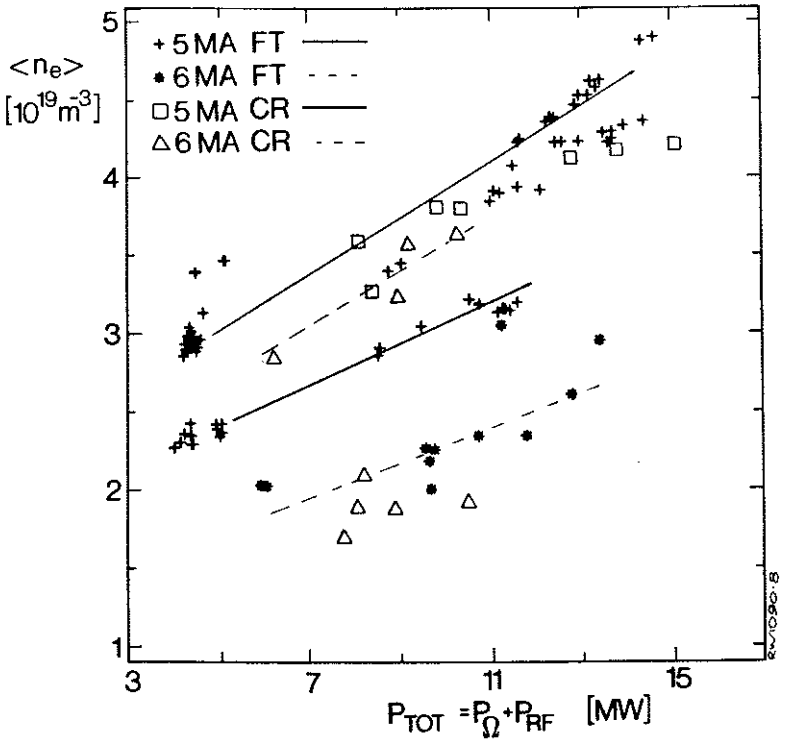

Fig. 8 Volume averaged density as a function of input power. The full and broken lines are drawn in order to facilitate the reading of the diagram.

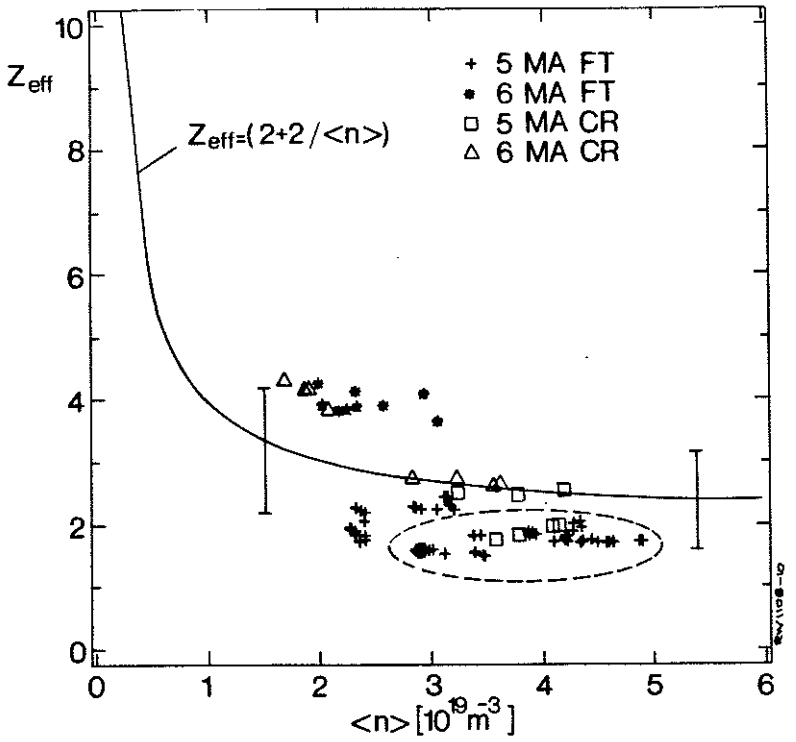

Fig. 9 Effective ion charge Z_{eff} versus volume averaged density. Line is the function $Z_{eff}=2+2/\langle n_e\rangle_{19}$, shown for comparison, which represents a previously published (Bickerton 1988) results. The bars indicate the spread in that dataset. The points within dashed line region correspond to 5MA FT and CR with systematic helium discharge cleaning.

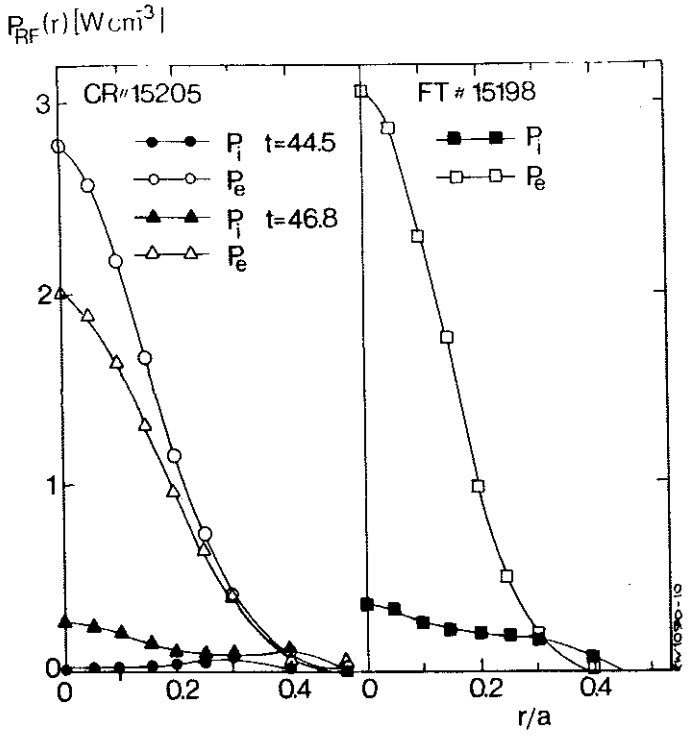

Fig. 10 Radial profiles of the redistributed RF power used in the transport calculation during CR and FT.

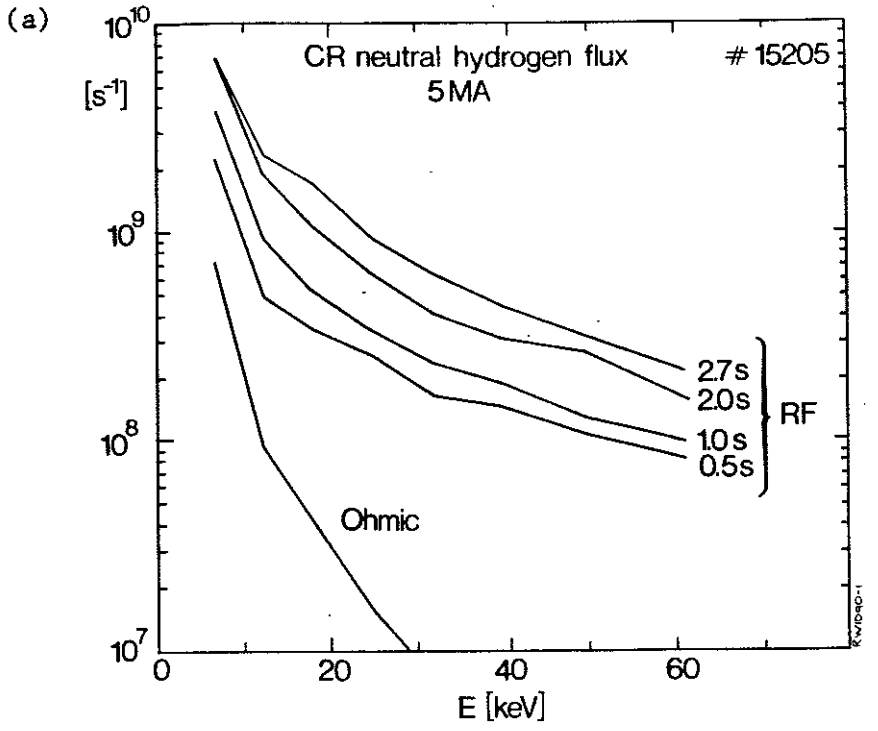

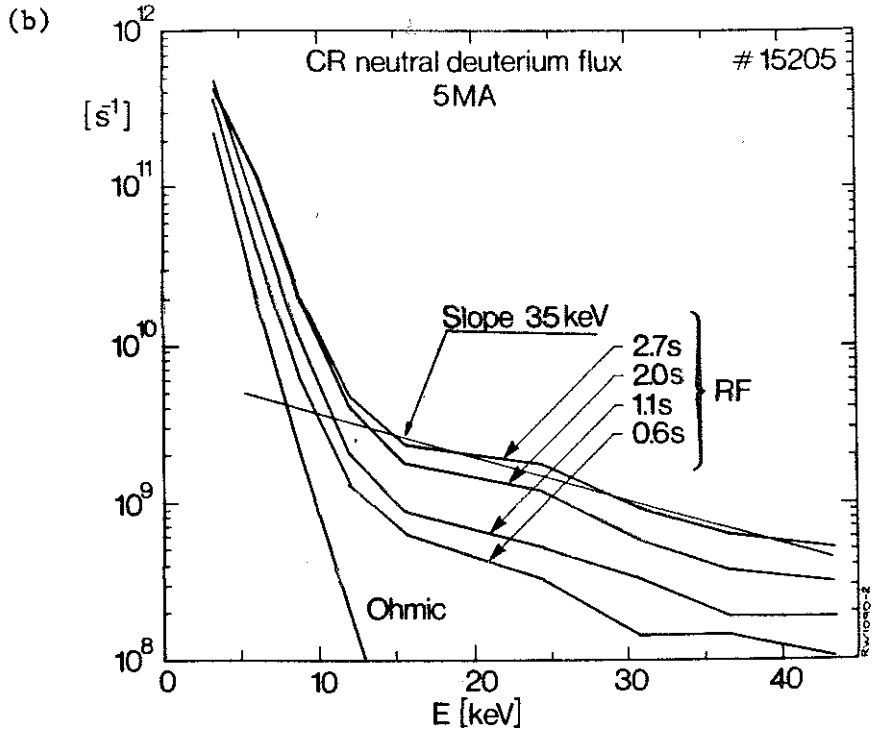

Fig. 11a,b Neutral hydrogen and deuterium flux spectra during the 5 MA CR discharge with 11 MW of RF power. The time corresponding to different spectra is measured from the onset of RF pulse.

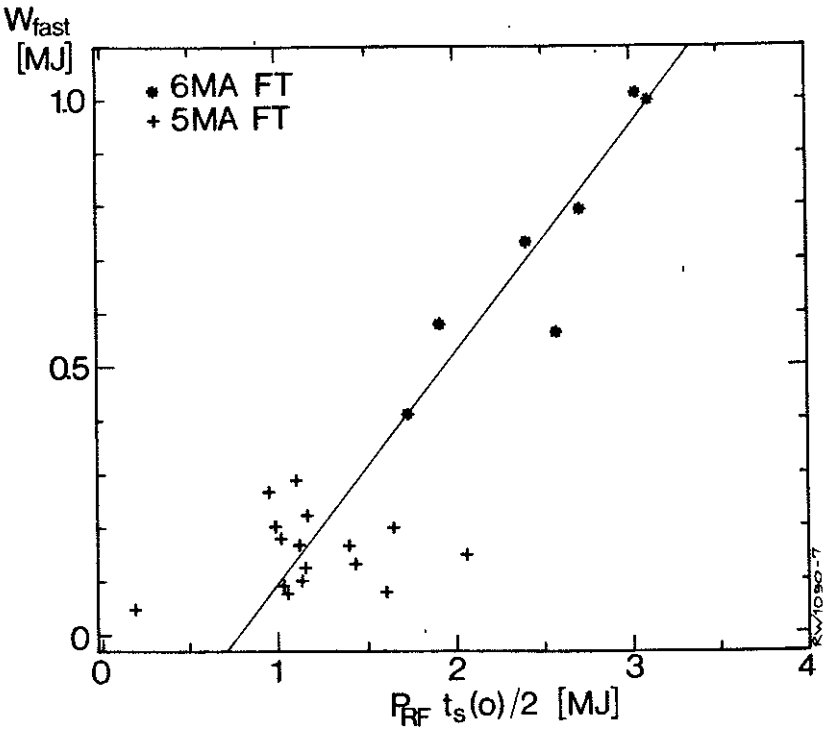

Fig. 12 Energy contained in fast particles estimated from the diamagnetic and kinetic energy contents plotted against the theoretical estimate. $t_s(0)$ represents the minority slowing-down time in the plasma centre.

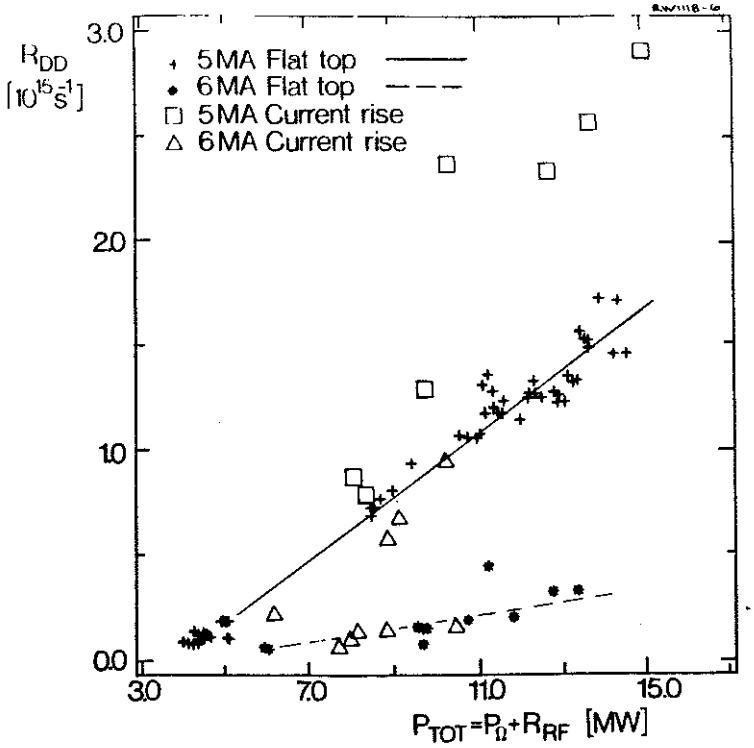

Fig. 13 Neutron yield as a function of power input. The full and broken lines are drawn in order to facilitate the reading of the diagram.

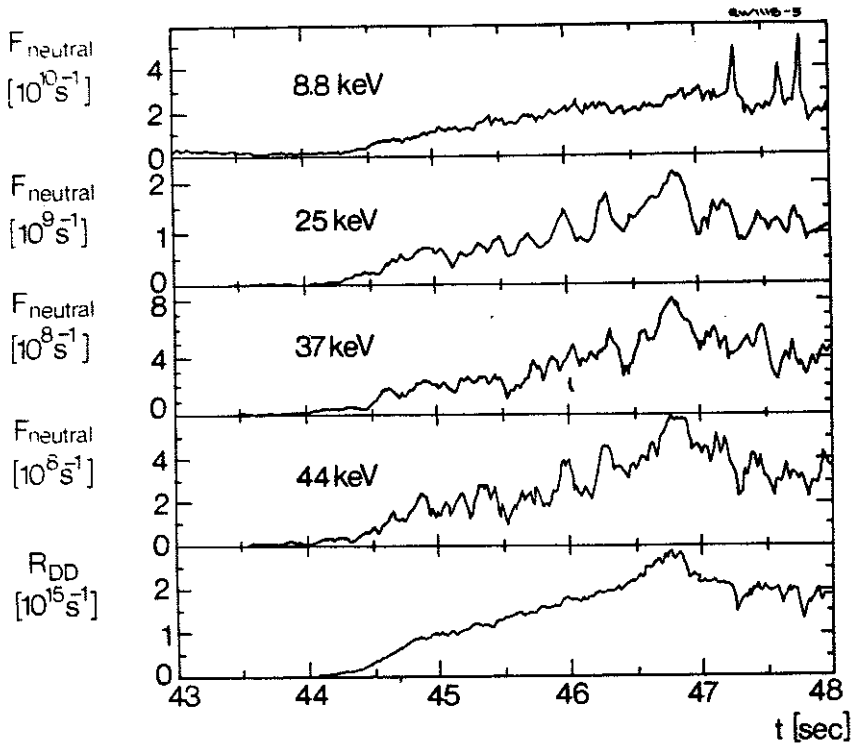

Fig. 14 Time evolution of the neutral deuterium fluxes at different energies and the neutron yield during a 5 MA CR discharge with 11 MW of RF power.

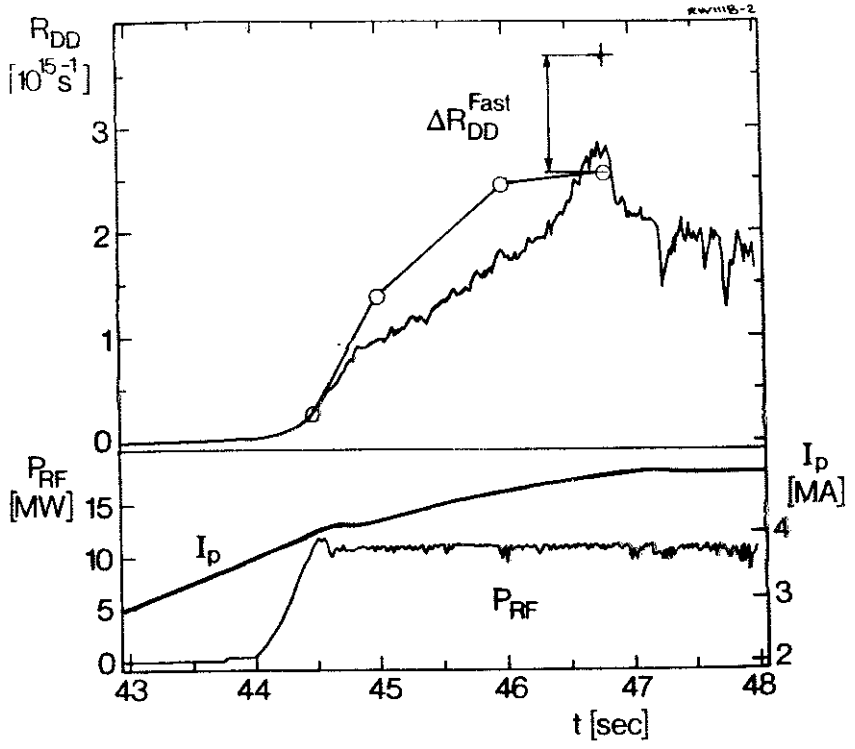

Fig. 15 Time evolution of measured and calculated neutron yield. Circles indicate the thermal contribution based on measured Z_{eff} ΔR_{DD}represents the contribution from the $2\omega_{CD}$ heating. Plasma current and RF power are also shown.

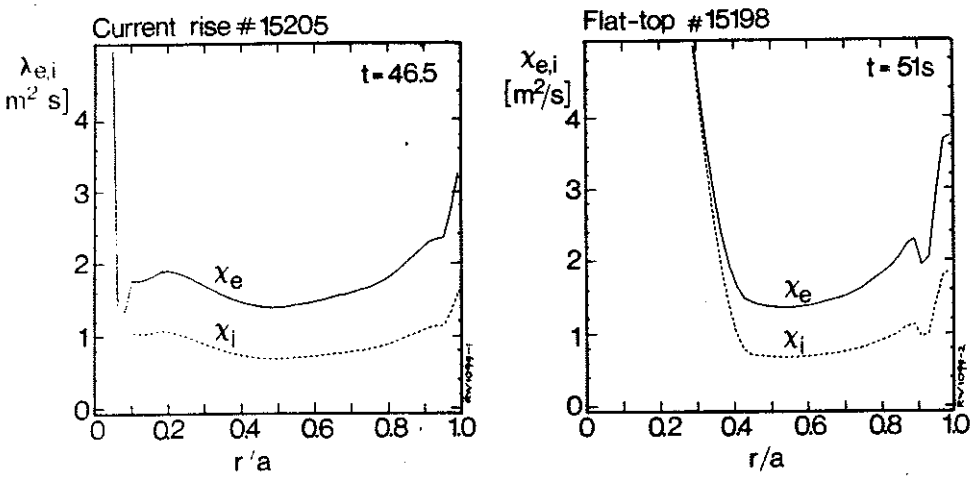

Fig. 16 Radial profiles of electron and ion thermal diffusivities $\chi_{e,i}$ for two discharges plotted in Fig. 5a,b. In the inner ($r/a < 0.1$) and outer ($r/a > 0.85$) regions the computations are not reliable.

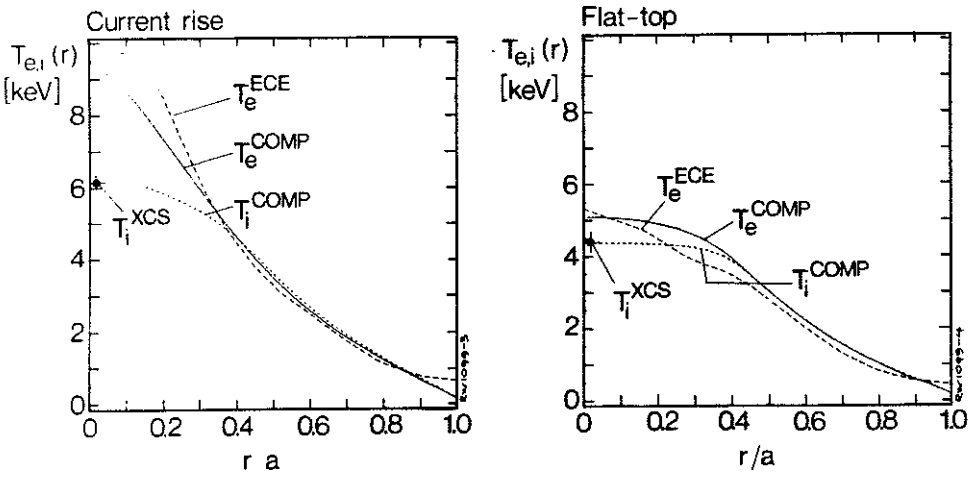

Fig. 17 Radial profiles of measured and computed electron and ion temperature profiles for two discharges plotted in Fig. 5a,b. Corresponding $\chi_{e,i}$'s are plotted in Fig. 16.